Computational Investigation of NO2 Adsorption and Reduction on Ceria and M−Doped CeO2 (111) (M = Mn, Fe) Surfaces

ARTICLE *in* THE JOURNAL OF PHYSICAL CHEMISTRY C · APRIL 2014

Impact Factor: 4.77 · DOI: 10.1021/jp412417e

2 AUTHORS, INCLUDING:

Hsin-Tsung Chen
Chung Yuan Christian University
78 PUBLICATIONS **704** CITATIONS

THE JOURNAL OF PHYSICAL CHEMISTRY C

Article

pubs.acs.org/JPCC

Computational Investigation of NO_2 Adsorption and Reduction on Ceria and M-Doped CeO_2 (111) (M = Mn, Fe) Surfaces

Yu-Huan Lu and Hsin-Tsung Chen*

Department of Chemistry and Center for Nanotechnology, Chung Yuan Christian University, Chungli 32023, Taiwan

Supporting Information

ABSTRACT: The interaction and mechanism for NO_2 reduction on ceria and M-doped CeO_2 (111) (M = Mn, Fe) surfaces have been studied by using periodic density functional theory calculations corrected with the on-site Coulomb interaction via a Hubbard term (DFT+U). Our calculations show that NO_2 adsorbs more strongly on the stoichiometric M-doped CeO_2 surfaces compared with the undoped surface, forming nitrate-like (NO_3^-) species with adsorption energies of −0.99 to −1.09 eV for CeO_2, −1.46 to −1.99 eV for $Ce_{0.875}Mn_{0.125}O_2$, and −1.32 to −1.64 eV for $Ce_{0.875}Fe_{0.125}O_2$. On the contrary, the adsorption of NO_2 is less stable at the oxygen vacancy site on the defective M-doped CeO_2 surfaces (−0.49 to −0.97 eV for $Ce_{0.875}Mn_{0.125}O_2$ and −0.70 to −1.35 eV for $Ce_{0.875}Fe_{0.125}O_2$) than on the defective undoped surface (−1.95 to −2.02 eV), forming nitrite-like species (NO_2^-). It is worth noting that the adsorption energies of NO_2 are proportional to the oxygen vacancy energies for stoichiometric surfaces, whereas they are disproportional to the oxygen vacancy energies for defective surfaces. For the reduction reaction in which NO_2 is reduced to NO and the defective CeO_2 and M-doped CeO_2 (111) surfaces are fully reoxidized, the reaction energy is exothermic for $CeO_{2-\delta}$, whereas it is endothermic for $Ce_{0.875}Mn_{0.125}O_{2-\delta}$ and $Ce_{0.875}Fe_{0.125}O_{2-\delta}$. The reaction energies depend on the oxygen vacancy formation energies, for which $Ce_{0.875}Mn_{0.125}O_2$ < $Ce_{0.875}Fe_{0.125}O_2$ < CeO_2. The vibrational frequency calculations as well as the Bader charge analysis are carried out to characterize the adsorbed species.

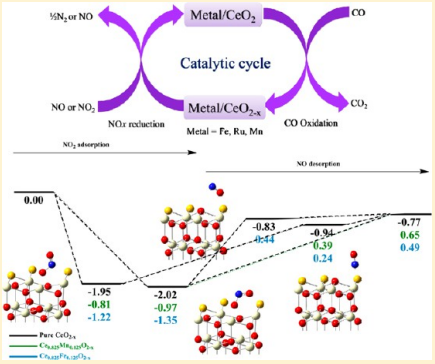

1. INTRODUCTION

Ceria (CeO_2) is a multifunction rare earth oxide with excellent physical and chemical properties and has been extensively explored for several advanced applications in the fields of heterogeneous catalysis, electrochemistry, photochemistry, and material science.[1−4] In general, CeO_2 is used in the three-way catalysts for reducing the emission of toxic pollutants (CO, NO_x, and hydrocarbon, etc.) from automobile exhaust due to its unique oxygen storage capacity associated with its rich oxygen vacancies.[5−9] Cerium oxide is used as a redox and support material in automotive catalysis. Recently, the use of ceria has been studied in the context of NO_x storage reduction used for lean-burn engines.[10,11] The redox reaction occurs via Mars−van Krevelen mechanism.[12] The CO molecule is oxidized to CO_2 molecule by taking oxygen from the cerium oxide and creating oxygen vacancies on the surfaces. Either an O_2 molecule from the gas phase can reoxidize the vacancies, forming O adspecies that then drive subsequent CO oxidation, or a molecule such as NO_2 or NO can be reduced with reoxidizing the vacancies to complete a full catalytic cycle for CO oxidation, NO_2 or NO reduction, and catalyst regeneration.[13] It is important to understand the reactivity and adsorption properties of this material by studying the interaction between molecules such as NO_2 and CO, with CeO_2-based surfaces. Previously, we had studied the interaction and mechanism for CO oxidation on metal-doped CeO_2 (111) surface by using DFT + U method.[14−16] In the present work, we extend our previous studies and investigate the adsorption and reduction of NO_2 on the ceria and Mn,Fe-doped CeO_2 (111) surfaces.

Reactions of NO_2 on ceria surfaces have been the subject of numerous investigations. Rodriguez et al.[17] and Berner et al.[18] studied the interaction of NO_2 with the (111) ceria surface and the (111) surface of ceria on a Pt support, respectively. Namai et al.[9] used AFM to study the interaction of NO_2 with a slightly reduced CeO_2(111) surface. UV photoemission spectroscopy (UPS) showed no evidence of NO_2 dissociation, while no change in surface structure was observed in AFM images, indicating that NO_2 does not interact with an oxidized surface. NO_2 was found to dissociate into NO on reduced ceria, coupled to a reduction in the intensity of the reduced Ce(III) peak in the UPS spectrum. It was found that NO_2 healed the oxygen vacancies on reduced ceria in AFM. These results demonstrate the necessity for the presence of reduced Ce(III) ions on the surface, which promote the breaking of one NO bond so that NO_2 dissociates into NO and O, with the latter leading to oxidation of the surface. Recently, in situ DRIFTS experiments have revealed that reaction of NO_2 with ceria results in nitrate and immediate nitrite formation.[19] Filtschew et al.[20] study the mechanism of NO_2 storage in ceria using in

Received: December 19, 2013
Revised: April 17, 2014
Published: April 17, 2014

   dx.doi.org/10.1021/jp412417e | J. Phys. Chem. C 2014, 118, 10043−10052

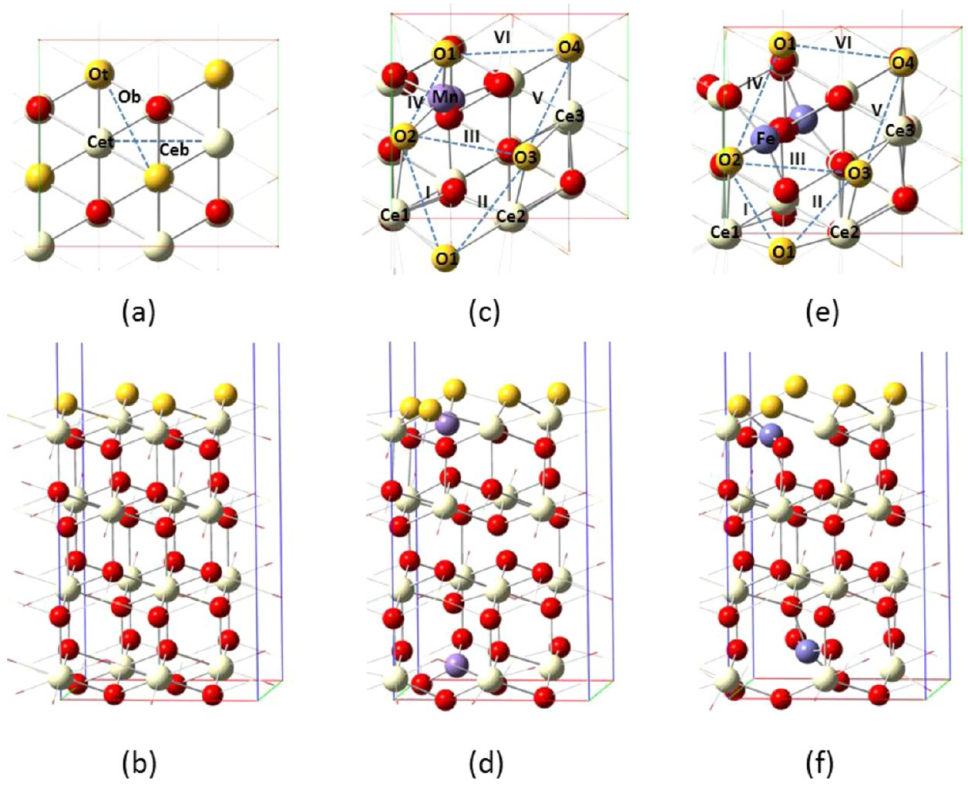

Figure 1. (a) Side and (b) top views of the CeO_2 (111) surface. **Cet**, **Ceb**, **Ot**, **Ob**, and **Oh** correspond to active sites for "Ce top", "Ce bridge", "O top", "O bridge", and "O hollow" sites, respectively. (c) Side and (d) top views of the $Ce_{0.875}Mn_{0.125}O_2$ (111) surface model. (e) Side and (f) top views of the $Ce_{0.875}Fe_{0.125}O_2$ (111) surface model. **I** (**IV**), **II**, **III**, **V**, and **VI** correspond to active sites for "O1−O2", "O1−O3", "O2−O3", "O3−O4", and "O1−O4" sites, respectively. Yellow, red, white, and cyanine blue spheres represent the top-layer O, O, Ce, and M (M = Mn, Fe) atoms, respectively. A rectangle represents the supercell used in this study.

situ Raman spectroscopy combined with FT-IR gas-phase analysis. They propose the following mechanism: exposure to NO_2 leads to the formation of different nitrate (free, bidentate, bridging) and nitrite species. Theoretically, Nolan et al.[21] and Galea et al.[22] have studied the adsorption of NO_2 on reduced (111), (110), and (100) surfaces of ceria, resulting in nitrite formation and partial ceria reoxidation, while NO_2 reduction to NO is accompanied by full ceria reoxidation. In addition, a GGA+U study of surface reduction and the adsorption of CO and NO_2 on CeO_2 (110) surface reported by Scanlon et al.[23] has demonstrated interactions involved in surface reduction and the adsorption of CO and NO_2 on the (110) ceria surface.

To the best our knowledge, molecular-level study of NO_2 reduction on metal-doped CeO_2 catalysts has not been previously investigated. In the present work, we attempt to address the NO_2 adsorption and the detailed reaction mechanisms of NO_2 reduction catalyzed by ceria and Mn,Fe-CeO_2 (111) surfaces that have used as catalysts for CO oxidation previously.[15,16]

2. COMPUTATIONAL METHODS

Spin-polarized density functional theory (DFT) plane-wave calculations as implemented in the Vienna ab initio simulation package (VASP)[24,25] with the projector-augmented wave method (PAW)[26] were performed. The electron exchange-correlation functional was treated within the generalized gradient approximation (GGA) with the Perdew−Wang 91 (PW91) exchange-correlation functional.[27−29] The calculations were carried out using the Brillouin zone sampled with (3 × 3 × 1) Monkhorst−Pack[30] mesh **k**-points grid with a cutoff energy of 400 eV, which allows convergence to 0.01 eV in the total energy. The DFT with the Hubbard U term (DFT+U) method[35] was applied to accurately correct the strong on-site Coulomb interactions of Ce_{4f} states to describe the localization of the Ce_{4f} states in the reduced ceria.[31−34,36] There is no general rule on a "correct" U value to describe the localized 4f orbitals of Ce. For example, Loschen et al.[37] proposed a well-balanced U value of 5 to 6 eV for LDA+U calculations and 2 to 3 eV for GGA+U calculations. Andersson et al.[38] clarified that the U value must satisfy the criteria of $U > 6$ eV for LDA calculations and $U > 5$ eV for GGA calculations to exactly predict the ground state of Ce_2O_x. The proposed U values seem to depend on the oxidation states of Ce and the functional used. As such, we chose $U = 6.3$ eV, which has been shown to work well for previous studies on the metal-doped ceria.[14−16,39−41]

For the surface model, we examined only the (111) surface to characterize the NO_2−ceria interactions because (111) surface is energetically the most stable among the low-index CeO_2 (111), (110), and (100) surfaces.[42−44] As shown in Figure 1, the slab model was a $p(\sqrt{3} \times 2)$ lateral cell with 12 atomic layers thick and a 15 Å vacuum gap in the direction perpendicular to the surface. To examine the effect of Mn and Fe cations for NO_2 reduction, for the (111) surface, one Ce atom of the outermost Ce layer on each side of the $p(\sqrt{3} \times 2)$ CeO_2 (111) slab was replaced by a Mn or Fe atom, giving an overall dopant concentration of 12.5%. The reduced systems were created by removing one oxygen atom resulting in an oxygen vacancy concentration of 6.25%. The bottom six layers of the surface model were fixed to the estimated bulk

dx.doi.org/10.1021/jp412417e | J. Phys. Chem. C 2014, 118, 10043−10052

Table 1. Interatomic Distances between Metal (Ce, Mn, Fe) and Oxygen Observed for Stoichiometric and Defective Surfaces[a]

	CeO_2 (111)	$CeO_{2-\delta}$ (111)	$Ce_{0.825}Mn_{0.125}O_2$ (111)	$Ce_{0.825}Mn_{0.125}O_{2-\delta}$ (111)	$Ce_{0.825}Fe_{0.125}O_2$ (111)	$Ce_{0.825}Fe_{0.125}O_{2-\delta}$ (111)
	2.37 (O1)	2.46 (O1)	2.67 (O1)	2.47 (O1)	2.25 (O1)	2.33 (O1)
Ce2−O (Å)	2.36 (O3)		2.41 (O3)		2.19 (O3)	
	2.36 (O4)	2.42 (O4)	2.28 (O4)	2.19 (O4)	2.34 (O4)	2.40 (O4)
average (Å)	2.36	2.44	2.45	2.33	2.26	2.37
	2.37 (O2)	2.40 (O2)	2.47 (O2)	2.48 (O2)	2.50 (O2)	2.40 (O2)
Ce3−O (Å)	2.37 (O3)		2.16 (O3)		2.15 (O3)	
	2.37 (O4)	2.42 (O4)	2.30 (O4)	2.34 (O4)	2.31 (O4)	2.31 (O4)
average (Å)	2.37	2.41	2.31	2.41	2.32	2.36
	2.37 (O1)	2.29 (O1)	1.83 (O1)	1.80 (O1)	3.46 (O1)	3.52 (O1)
M−O (Å)	2.36 (O2)	2.26 (O2)	1.89 (O2)	1.83 (O2)	1.80 (O2)	1.84 (O2)
(M = Ce, Mn, Fe)	2.36 (O3)		3.56 (O3)		3.63 (O3)	
average (Å)	2.36	2.28	2.43	1.82	2.96	2.68

[a]Labels are defined in Figure 1.

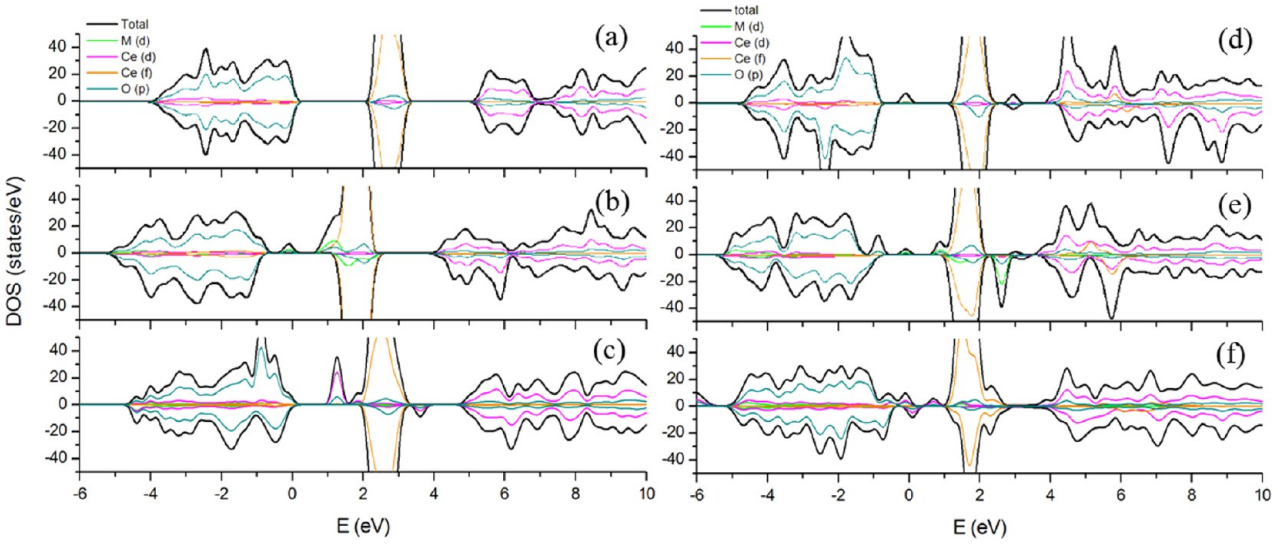

Figure 2. Density of states and local density of states for stoichiometric (a) CeO_2, (b) $Ce_{0.875}Mn_{0.125}O_2$, and (c) $Ce_{0.875}Fe_{0.125}O_2$ surfaces and for defective (d) $CeO_{2-\delta}$, (e) $Ce_{0.875}Mn_{0.125}O_{2-\delta}$, and (f) $Ce_{0.875}Fe_{0.125}O_{2-\delta}$ surfaces. The energy at E = 0 eV represents the Fermi energy.

parameters, while the remaining layers were fully optimized. The adsorption energies were calculated by the equation: $\Delta E_{ads} = E[\text{surface-adsorbate}] - E[\text{surface}] - E[\text{adsorbate}]$, where E[surface-adsorbate], E[surface], and E[adsorbate] are the calculated electronic energies of adsorbed species on the surface, the bare surface, and the adsorbate in the gas phase, respectively. The climbing image nudged elastic band (CI-NEB) method[45,46] was applied to map out MEPs after locating plausible local minima. All transition states were verified by the number of imaginary frequencies (NIMG) with NIMG = 1. The charge density difference was calculated using the expression: $\Delta\rho_{diff} = \rho[\text{surface + adsorbate}] - \rho[\text{surface}] - \rho[\text{adsorbate}]$, where ρ[surface + adsorbate], ρ[surface], and ρ[adsorbate] are the charge density of adsorbed species on the surface, the bare surface, and the adsorbate, respectively.

3. RESULTS AND DISCUSSION

3.1. Stoichiometric Ceria and Doped CeO_2 Surfaces.

To ensure the reliability of the computational results, we first predicted bulk lattice constants and compared them with the experimental values. The predicted lattice constants for undoped, Mn-doped, and Fe-doped ceria are 5.45, 5.39, and 5.42 Å, respectively, which is in agreement with the experimental values of 5.41,[47] 5.41,[48] and 5.42 Å.[49] The optimized stoichiometric CeO_2 (111) surface has the Ce−O bond length equal to 2.36 to 2.37 Å, as shown in Table 1. The relaxed structures of M-doped CeO_2 (111) surfaces in which two Ce atoms are replaced by two M atoms are shown in Figure 1b,c for M = Mn and Fe, respectively, while optimized M-doped CeO_2 (111) surfaces show geometric distortions of the oxygen lattice. For the $Ce_{0.875}Mn_{0.125}O_2$ surface, the Mn atom has relaxed to form short Mn−O bond distances of 1.83 (Mn−O1) and 1.89 (Mn−O2) Å and long Mn−O3 bond distance of 3.56 Å with Ce2−O bonds of 2.67 (O1), 2.41 (O3), and 2.28 (O4) Å and Ce3−O bonds of 2.47 (O2), 2.16 (O3), and 2.30 (O4) Å; see Table 1. In the $Ce_{0.875}Fe_{0.125}O_2$ structure, the Fe atom has relaxed to form short Fe−O bond distances of 1.80 Å and two long Fe−O bond distances of 3.46 (O2) and 3.63 (O3) Å with Ce2−O bonds of 2.25 (O1), 2.19 (O3), and 2.34 (O4) Å and Ce3−O bonds of 2.50 (O2), 2.15 (O3), and 2.31 (O4) Å. (See Table 1.)

The oxygen vacancy formation is described by the reaction $Ce_{1-x}M_xO_2 \rightarrow Ce_{1-x}M_xO_{2-\delta} + 1/2O_2$. The oxygen vacancy formation energy, E_f, was computed according to eq 1

$$E_f = E(Ce_{1-x}M_xO_{2-\delta}) + 1/2E(O_2) - E(Ce_{1-x}M_xO_2) \quad (1)$$

dx.doi.org/10.1021/jp412417e | J. Phys. Chem. C 2014, 118, 10043−10052

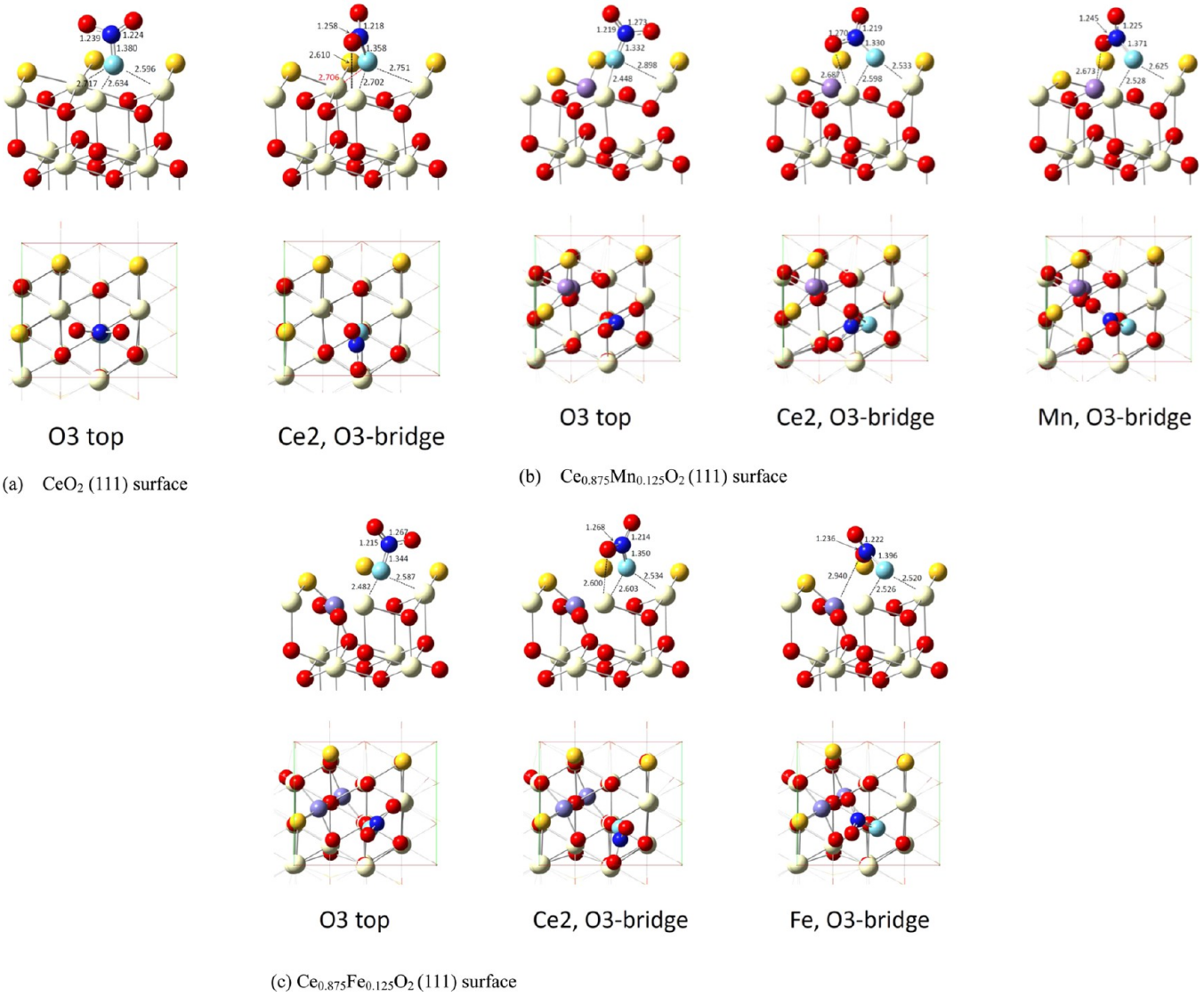

Figure 3. Side view and top view for the optimized structures of NO_2 chemisorbed on the stoichiometric surfaces. NO_2 chemisorption on (a) CeO_2 (111) surface, (b) $Ce_{0.875}Mn_{0.125}O_2$ (111) surface, and (c) $Ce_{0.875}Fe_{0.125}O_2$ (111) surface.

where $E(Ce_{1-x}M_xO_2)$ indicates the energy of the bulk or surface $Ce_{1-x}M_xO_2$, $E(O_2)$ is the energy of a gas-phase O_2, and $E(Ce_{1-x}M_xO_{2-\delta})$ is the energy of the bulk in the presence of one oxygen vacancy. In the present study, we only show the formation of oxygen vacancy neighboring the metal dopant because the required energy for the vacancy further away from metal dopant is close to the undoped CeO_2. The calculated E_f values are 3.20, 0.73, and 1.04 eV for undoped, Mn-, and Fe-doped CeO_2 bulk, respectively. The formation energies of surface O vacancy are calculated to be 2.08, 0.55, and 0.68 eV for undoped, Mn-, and Fe-doped CeO_2 surface, respectively. The smaller E_f indicates that Mn- and Fe-doped ceria show higher OSC property than CeO_2, which is consistent with the experimental results.[49] The removal of an oxygen results in a significant distortion around the three anions originally coordinated to the oxygen (O3). As presented in Table 1, the surface Ce−O distances in defective CeO_2 (111) surface are calculated to be 2.44 (Ce2−O), 2.41 (Ce3−O), and 2.28 (Ce−O) Å on average. For the $Ce_{0.875}Mn_{0.125}O_{2-x}$ surface, the Mn−O distances are calculated to be 1.80 (Mn−O1) and 1.83 (Mn−O2) Å with Ce2−O bonds of 2.47 (O1) and 2.19 (O4) Å and Ce3−O bonds of 2.48 (O2) and 2.34 (O4) Å (Table 1). In the $Ce_{0.875}Fe_{0.125}O_{2-x}$ structure, the Fe−O bond lengths are calculated to be 1.82 (O2) and 3.52 (O1) Å, with Ce2−O distances of 2.33 (O1) and 2.40 (O4) Å and Ce3−O distances of 2.40 (O2) and 2.31 (O4) Å (Table 1).

The features of the electronic density of states (DOS) and local density of states (LDOS) for above structures are shown in Figure 2. The stoichiometric CeO_2 (111) surface is well known to be an insulator. When a ceria surface is reduced, a gap state appears between the valence band and the unoccupied Ce 4f states (Figure 2). The gap state is mainly composed of Ce 4f states, which has also been seen with other DFT+U calculations.[21,23,50]

3.2. Adsorption and Reaction of NO_2 on Stoichiometric Ceria and M-Doped CeO_2 (111) Surfaces. The interactions between NO_2 and stoichiometric CeO_2 and M-doped CeO_2 (111) surfaces were investigated using DFT+U calculations first. Plausible intermediates for the NO_2−CeO_2 or NO_2−$Ce_{0.875}M_{0.125}O_2$ interactions were initially optimized by placing a single NO_2 molecular at different active sites on the (111) surface, as shown in Figure 1. The NO_2 interactions with

dx.doi.org/10.1021/jp412417e | J. Phys. Chem. C 2014, 118, 10043−10052

Table 2. Adsorption Energy (eV) and Calculated Frequencies (cm^{-1}) of NO_2 on Stoichiometric $CeO_2(111)$, $Ce_{0.825}Mn_{0.125}O_2(111)$, and $Ce_{0.825}Fe_{0.125}O_2(111)$ Surfaces[a,b]

adsorption site	CeO_2 (eV)	frequency	$Ce_{0.875}Mn_{0.125}O_2$	frequency	$Ce_{0.825}Fe_{0.125}O_2$	frequency
Physisorption						
O3 top	−0.11 (−0.07)[c]	1640, 1314, 722	−0.23 (−0.06)	1649, 1318, 715		
Ce2, O3-bridge	−0.16 (−0.07)	1644, 1307, 711	−0.12 (−0.07)	1645, 1304, 711	−0.05 (−0.09)	1664, 1323, 720
Chemisorption						
O3 top (η^1-N)	−0.99 (−1.31)[c]	1599, 1261	−1.95 (−0.80)	1563, 1212	−1.64 (−0.73)	1586, 1212
Ce2, O3-bridge (μ^2-N,O)	−1.09 (−1.10)	1587, 1237	−1.99 (−0.79)	1572, 1225	−1.56 (−0.76)	1595, 1209
M, O3-bridge (μ^2-N,O); M = Mn, Fe			−1.46 (−0.83)	1570, 1241	−1.32 (−0.80)	1596, 1250

[a]Calculated frequencies of a gas-phase NO_2 are 1702, 1394, and 767 cm^{-1}, while the experimental values are 1618, 1318, and 750 cm^{-1}. [b]Experimental frequencies of nitrate species on CeO_2 surface are 1540−1599 and 1170−1270 cm^{-1}. [c]Values in parentheses are effective charges that are calculated by the Bader analysis program.

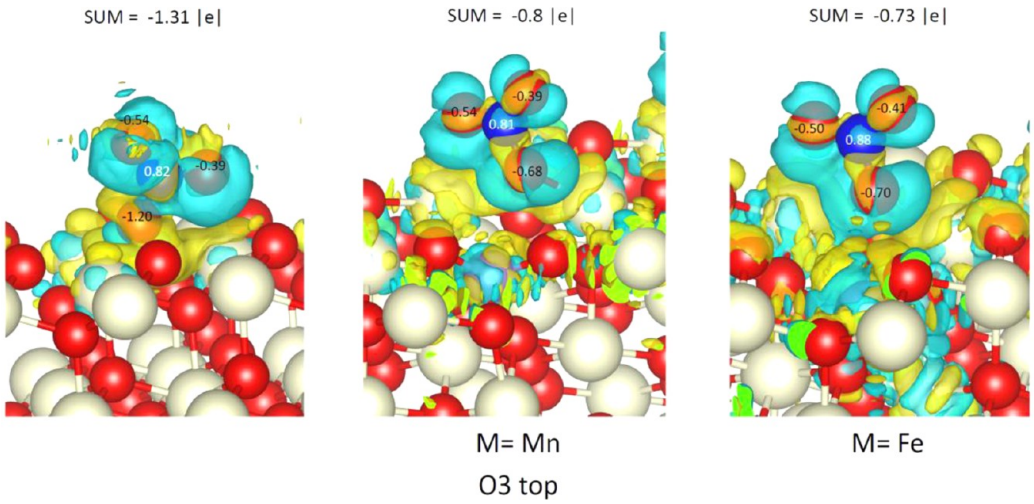

Figure 4. Illustration of charge-density difference for NO_2 chemisorption (nitrate-like species) at O3 top site on (a) CeO_2 (111) surface, (b) $Ce_{0.875}Mn_{0.125}O_2$ (111) surface, and (c) $Ce_{0.875}Fe_{0.125}O_2$ (111) surface. $\Delta\rho_{diff}$ isosurfaces were calculated at 0.05 $bohr^{-3}$. The values are effective charges that are calculated by the Bader analysis program.

the surface can be divided into physisorption and chemisorption. The optimized configurations of NO_2 physisorption and NO_2 chemisorption are presented in Figure S1 (Supporting Information) and Figure 3, respectively. Table 2 displays the relative adsorption energies and calculated frequencies. NO_2 physisorption is observed at the oxygen and metal center (Ce, Mn, and Fe) sites with adsorption energies of −0.11 to −0.16, −0.12 to −0.23, and −0.05 eV for NO_2−CeO_2, NO_2−$Ce_{0.875}Mn_{0.125}O_2$, and NO_2−$Ce_{0.875}Fe_{0.125}O_2$, respectively. The distances of N−O_{surf} and N−Ce_{surf} are 2.583 to 2.727 and 2.972 to 2.978 Å. (See Figure S1 in the Supporting Information.) As seen in Figure 3, NO_2 prefers to bind to the oxide anions via the nitrogen (η^1-N) or bind to O and metal centers via bidentate adsorption mode (μ^2-N,O), leading to NO_2 chemisorption and formation of nitrate-like species (NO_3^-). The lengths of the N−O_{surf} bond for the monodentate adsorption modes (η^1-N) are 1.380, 1.332, and 1.344 Å for NO_2−CeO_2, NO_2−$Ce_{0.875}Mn_{0.125}O_2$, and NO_2−$Ce_{0.875}Fe_{0.125}O_2$, respectively (see Figure 3), which are elongated compared with that of a free NO_3^- molecule (1.18 Å). The lengths of the N−O_{surf} and O−M_{surf} bonds for the bidentate adsorption modes (μ^2-N,O) are 1.358, 1.330 to 1.371, and 1.350 to 1.396 Å and 2.610, 2.673 to 2.687, and 2.600 to 2.904 Å (see Figure 3). The adsorption energies for NO_3^--like species on the CeO_2, $Ce_{0.875}Mn_{0.125}O_2$, and $Ce_{0.875}Fe_{0.125}O_2$ (111) surfaces are −0.99 to −1.09, −1.46 to − 1.99, and −1.32 to −1.64 eV. A Bader charge analysis gives net charges of −1.10 to −1.31, −0.79 to − 0.83, and −0.73 to −0.80 *e* (see Table 2 and Figure 4) for the nitrate-like species on the CeO_2, $Ce_{0.875}Mn_{0.125}O_2$ and $Ce_{0.875}Fe_{0.125}O_2$ (111) surfaces, respectively, and which seem to be a reasonable value for a bound NO_3^- ion. The vibrational frequencies for the adsorbed species on the stoichiometric (111) surfaces are summarized in Table 2. The predicted vibrational frequencies at the region of 1640−1664, 1304−1323, and 711−722 cm^{-1} are attributed to NO_2 physisorption, where the values are close to that of a gas-phase NO_2 molecule (the calculated frequency values of 1702, 1394, and 767 cm^{-1} and the experimental values of 1618, 1318, and 750 cm^{-1}), as shown in Table 2. The predicted frequencies of nitrate-like species (1563−1599 and 1209−1261 cm^{-1}) are in close agreement with the experimental value, 1540−1599 and 1170−1270 cm^{-1}.[20] The decomposition process producing defective surface and a gas-phase NO_3 molecule from NO_2−CeO_2, NO_2−$Ce_{0.875}Mn_{0.125}O_2$, and NO_2−$Ce_{0.875}Fe_{0.125}O_2$ requires very high energies of 2.85−2.95, 1.91−2.44, and 1.93−2.25 eV. The final product defective surface and NO_3(g) is 1.86, 0.45, and 0.61 eV above the initial reactants in energy, indicating that it is difficult to emit NO_3(g) with an oxygen vacancy formation from the surfaces. The results are consistent with the experiment,[20] which shows that a temperature of 200 °C is needed to form free nitrate.

3.3. Adsorption and Reaction of NO_2 on Defective Ceria and M-doped CeO_2 (111) Surfaces. Dissociation of NO_2 to NO will not occur on the stoichiometric surface of

dx.doi.org/10.1021/jp412417e | J. Phys. Chem. C 2014, 118, 10043−10052

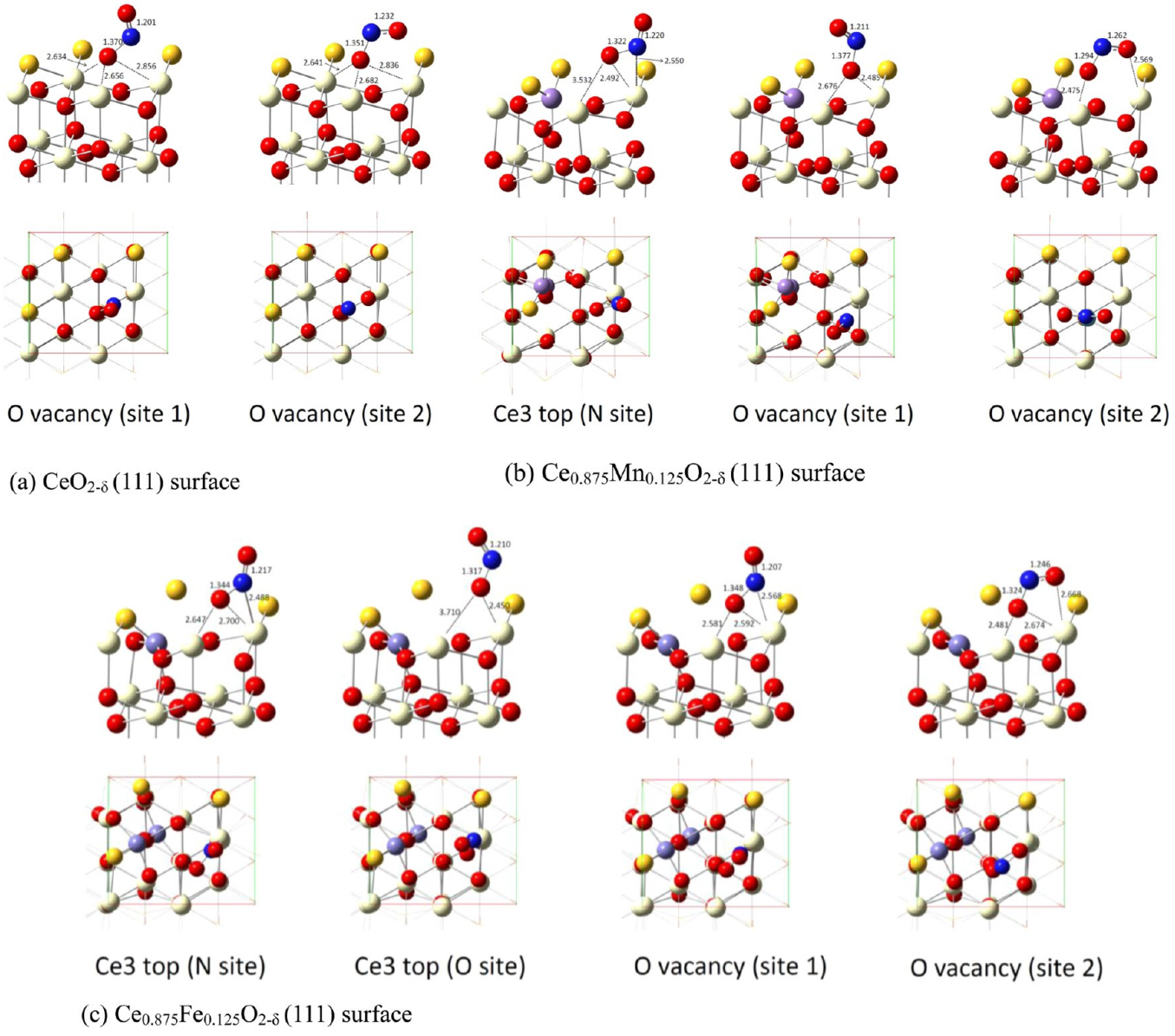

Figure 5. Side view and top view for the optimized structures of NO_2 chemisorbed on the defective surfaces. NO_2 chemisorption on (a) $CeO_{2-\delta}$ (111) surface, (b) $Ce_{0.875}Mn_{0.125}O_{2-\delta}$ (111) surface, and (c) $Ce_{0.875}Fe_{0.125}O_{2-\delta}$ (111) surface.

Table 3. Adsorption Energy (eV) and Calculated Frequencies (cm^{-1}) of NO_2 on Defective CeO_{2-x}(111), $Ce_{0.825}Mn_{0.125}O_{2-x}$(111), and $Ce_{0.825}Fe_{0.125}O_{2-x}$(111) Surfaces[a,b]

adsorption site	$CeO_{2-\delta}$ (eV)	frequency	$Ce_{0.875}Mn_{0.125}O_{2-\delta}$	frequency	$Ce_{0.825}Fe_{0.125}O_{2-\delta}$	frequency
			Physisorption			
Ce3 top (O site)			−0.15 (−0.24)[c]	796, 996, 1603	−0.27 (−0.26)	710, 1175, 1549
Ce3 top (N site)					−0.27 (−0.29)	952, 1130, 1579
			Chemisorption			
Ce3 top (O site; η^2-O,N)					−0.70 (−0.49)	875, 1467
Ce3 top (N site; η^2-N,O)			−0.49 (−0.73)	727, 1542	−1.00 (−0.74)	720, 1546
O vacancy (site 1; μ^2-N,O)	−1.95 (−0.83)[c]	701, 1701	−0.81 (−0.80)	892, 1556	−1.22 (−0.72)	928, 1602
O vacancy (site 2; μ^2-N,O)	−2.02 (−0.81)	762, 1454	−0.97 (−0.78)	783, 1310	−1.35 (−0.75)	796, 1387
			NO Formation			
Ce3 top (O site)	−0.83 [−0.06][d]				0.44 [−0.05]	1906
Ce3 top (N site)	−0.94 [−0.18]	1874	0.39 [−0.26]	1854	0.24 [−0.24]	1906

[a]Calculated frequencies of a gas-phase NO are 1990 cm^{-1}, while the experimental values are 1904 cm^{-1}. [b]Experimental frequencies of nitrite species on defective CeO_2 surface are 1484−1716 cm^{-1}. [c]Values in parentheses ( ) are effective charges. [d]Values in square brackets [ ] are the calculated adsorption energies of NO on stoichiometric surfaces.

dx.doi.org/10.1021/jp412417e | J. Phys. Chem. C 2014, 118, 10043−10052

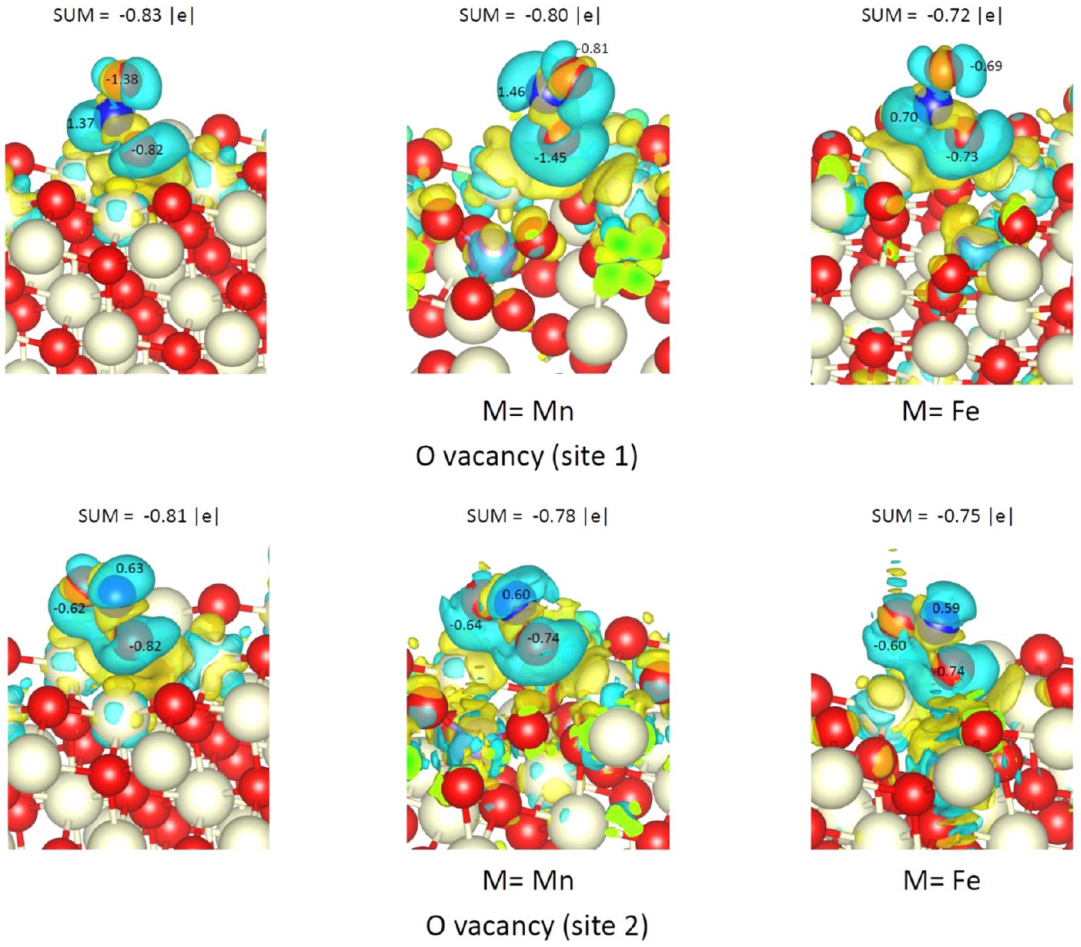

Figure 6. Illustration of charge-density difference for NO_2 chemisorption (nitrite-like species) at O vacancy site on (a) $CeO_{2-\delta}$ (111) surface, (b) $Ce_{0.875}Mn_{0.125}O_{2-\delta}$ (111) surface, and (c) $Ce_{0.875}Fe_{0.125}O_{2-\delta}$ (111) surface. $\Delta\rho_{diff}$ isosurfaces were calculated at 0.05 bohr^{-3}. The values are effective charges that are calculated by the Bader analysis program.

CeO_2, $Ce_{0.875}Mn_{0.125}O_2$ and $Ce_{0.875}Fe_{0.125}O_2$ (111) surfaces instead of the formation of stable NO_3^--like species, requiring surface prereduction to produce reactive O vacancy sites. In the vacancy adsorption mode, the NO_2 bonds to the $CeO_{2-\delta}$ and M-doped $CeO_{2-\delta}$ (111) surfaces in several different configurations by utilizing its O and N atoms, leading to the products of NO_2 physisorption and chemisorption. The optimized configurations of NO_2 physisorption and NO_2 chemisorption are presented in Figure S2 (Supporting Information) and Figure 5, respectively. Table 3 displays the relative adsorption energies and calculated frequencies. NO_2 physisorption is observed only at the Ce top sites of $Ce_{0.875}Mn_{0.125}O_{2-\delta}$ and $Ce_{0.875}Fe_{0.125}O_{2-\delta}$ surfaces with adsorption energies of −0.15 eV (N atom of NO_2 bond to Ce) for the $Ce_{0.875}Mn_{0.125}O_{2-\delta}$ surface and −0.27 (N atom of NO_2 bond to Ce) and −0.27 eV (O atom of NO_2 bond to Ce) for the $Ce_{0.875}Fe_{0.125}O_{2-\delta}$. The distance of O−$Ce_{surf}$ is 2.471 Å for NO_2−$Ce_{0.875}Mn_{0.125}O_{2-\delta}$ and the distances of O−Ce_{surf} and N−Ce_{surf} are 2.668 and 2.804 Å for NO_2−$Ce_{0.875}Fe_{0.125}O_{2-\delta}$. (See Figure S2 in the Supporting Information.) The NO_2 molecule adsorbs at the oxygen vacancy site through one of its oxygen atoms, leading to two bidentate adsorption modes: μ^2-N,O on M, vac and μ^2-O,O on M, vac. (See Figure 5.) We denote the oxygen atom of NO_2 occupying the pre-exiting vacancy site as O_V and the other oxygen atom as O_N. Adsorption of NO_2 on the defective surfaces results in significant elongation of the N−O_V bond distance from its gas-phase value of 1.203 Å to 1.370 (site 1: μ^2-N,O on M, vac) and 1.351 (site 2: μ^2-O,O on M, vac) Å on the $CeO_{2-\delta}$ (111) surface, 1.322, 1.377, and 1.294 Å on the $Ce_{0.875}Mn_{0.125}O_{2-\delta}$ (111) surface, and 1.344, 1.317, 1.348, and 1.294 Å on the $Ce_{0.875}Fe_{0.125}O_{2-\delta}$ (111) surface. The N−O_N bond distance changes only slightly, being 1.232 Å (CeO_{2-x} surface), 1.220, 1.211, and 1.262 Å ($Ce_{0.875}Mn_{0.125}O_{2-\delta}$ surface), and 1.217, 1.210, 1.207, and 1.246 Å ($Ce_{0.875}Fe_{0.125}O_{2-\delta}$ surface). The adsorption energies of bidentate μ^2-N,O on M, vac are calculated to be −1.95, −0.89, and −1.23 eV for $CeO_{2-\delta}$, $Ce_{0.875}Mn_{0.125}O_{2-\delta}$, and $Ce_{0.875}Fe_{0.125}O_{2-\delta}$ (111) surfaces, respectively, while the adsorption energies of bidentate μ^2-O,O on M, vac are predicted to be −2.02, −0.97, and −1.35 eV. Interestingly, other NO_2 chemisorption can be found for the defective M-doped CeO_2 (111) surfaces. The NO_2 molecule adsorbs at the Ce top site through its nitrogen atom, leading to the bidentate adsorption modes of η^2-N,O on Ce3 cation with adsorption energy of −0.49 eV for $Ce_{0.875}Mn_{0.125}O_{2-\delta}$ and the bidentate adsorption modes of η^2-N,O (through nitrogen atom of NO_2) and η^2-O,N (through oxygen atom of NO_2) on Ce3 cation with adsorption energies of −1.00 and −0.70 eV for $Ce_{0.875}Fe_{0.125}O_{2-\delta}$. (See Figure 5.) The N−$O_{Ce}$ bond distances elongate to 1.322 (η^2-N,O for $Ce_{0.875}Mn_{0.125}O_{2-\delta}$), 1.344 ($\eta^2$-N,O for $Ce_{0.875}Fe_{0.125}O_{2-\delta}$) and 1.317 ($\eta^2$-O,N for $Ce_{0.875}Fe_{0.125}O_{2-\delta}$) Å. A Bader charge analysis gives net charges

dx.doi.org/10.1021/jp412417e | J. Phys. Chem. C 2014, 118, 10043−10052

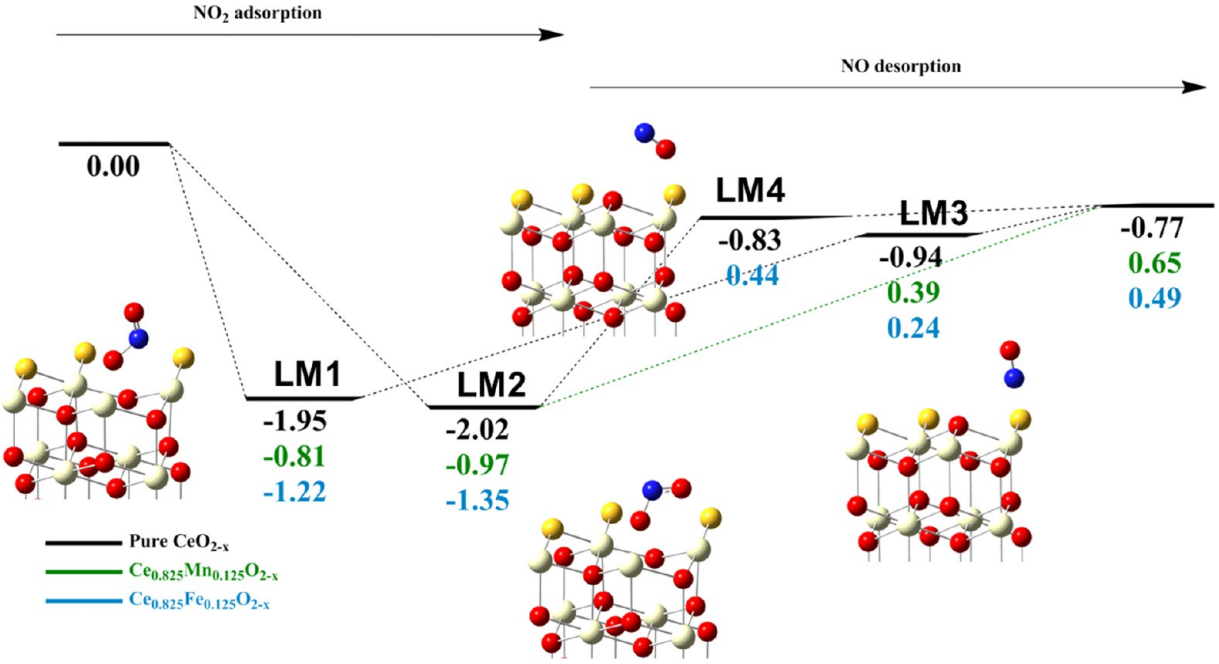

Figure 7. Calculated potential energy diagram for NO_2 reduction on $CeO_{2-\delta}$ (111), $Ce_{0.875}Mn_{0.125}O_{2-\delta}$ (111), and $Ce_{0.875}Fe_{0.125}O_{2-\delta}$ (111) surface. The unit of energy is electronvolts.

of −0.81 to −0.83, −0.73 to − 0.80, and −0.72 to −0.75 *e* (see Table 3 and Figure 6) for the NO_2 chemisorption on $CeO_{2-\delta}$, $Ce_{0.875}Mn_{0.125}O_{2-\delta}$, and $Ce_{0.875}Fe_{0.125}O_{2-\delta}$ (111) surfaces. The net charges of NO_2 chemisorption seem to be a reasonable value for a bound NO_2^- ion. Accordingly, those are assigned to nitrite-like species. The vibrational frequencies for the adsorbed species on the defective (111) surfaces were estimated as summarized in Table 3. The predicted vibrational frequencies at the region of 710−752, 996−1175, and 1549−1603 cm^{-1} are attributed to the physisorbed NO_2 for which the vibrational frequency values are close to those of a gas-phase NO_2 molecule (750, 1318, and 1618 cm^{-1}). The predicted N−O frequencies of nitrite-like species (1387−1701 cm^{-1}) are in close agreement with the experimental values, 1484−1716 cm^{-1}.[18]

The reduction of NO_2 catalyzed by $CeO_{2-\delta}$ and $Ce_{0.875}M_{0.125}O_{2-\delta}$ (111) has been addressed, and the calculated reaction mechanism is illustrated in Figure 7, including the following elementary steps

$$NO_{2(g)} + CeO_{2-\delta}/Ce_{0.875}M_{0.125}O_{2-\delta} \rightarrow [NO_{2(ads)}]^-[CeO_{2-\delta}/Ce_{0.875}M_{0.125}O_{2-\delta}]^+$$

$$[NO_{2(ads)}]^-[CeO_{2-\delta}/Ce_{0.875}M_{0.125}O_{2-\delta}]^+ \rightarrow [NO_{(ads)}][CeO_2/Ce_{0.875}M_{0.125}O_2]$$

$$[NO_{(ads)}][CeO_2/Ce_{0.875}M_{0.125}O_2] \rightarrow NO_{(g)} + CeO_2/Ce_{0.875}M_{0.125}O_2$$

First, the NO_2 adsorbs bidentately at M, vac site forming two surface−adsorbate modes, μ^2-N,O (**LM1**) and μ^2-O,O (**LM2**) intermediates; see Figure 7. In the surface−adsorbate, $[NO_{2(ads)}]^-[CeO_{2-\delta}/Ce_{0.875}M_{0.125}O_{2-\delta}]^+$, an electron has been transferred from reduced ceria to the NO_2 molecule, accompanied by the partially reoxidized surface. The **LM1** and **LM2** are calculated to be −1.95, −0.81, and −1.22 eV and −2.02, −0.97, and −1.35 eV with respect to reactants for $CeO_{2-\delta}$, $Ce_{0.875}Mn_{0.125}O_{2-\delta}$, and $Ce_{0.875}Fe_{0.125}O_{2-\delta}$ (111) surfaces, respectively, showing that the formation of the surface−adsorbate complex is favorable. The following deoxygenation of $NO_{2(ads)}$ occurs without any activation energy, leading to $[NO_{(ads)}][CeO_2/Ce_{0.875}M_{0.125}O_2]$ (**LM3** and **LM4**). It should be noted that we cannot find **LM4** configuration for the $Ce_{0.875}M_{0.125}O_{2-\delta}$ system. This dissociation process is endothermic and requires 1.01 to 1.79 eV, which is consistent with the temperatures needed for the reaction to occur.[17,18] The desorption of $NO_{(ads)}$ in **LM3** and **LM4** results in the full surface reoxidation. In view of the interactions between NO molecule and the stoichiometric surfaces, NO molecule is weakly bound to the surface with slight desorption energies of 0.05 to 0.26 eV; see Figure 7. The overall $NO_{2(g)}$ + $CeO_{2-\delta}/Ce_{0.875}M_{0.125}O_{2-\delta}$ → $NO_{(g)}$ + $CeO_2/Ce_{0.875}M_{0.125}O_2$ reaction is exothermic with reaction energy of −0.77 eV for $CeO_{2-\delta}$ surface and endothermic with reaction energies of 0.65 eV for the $Ce_{0.875}Mn_{0.125}O_{2-\delta}$ surface and 0.49 eV for $Ce_{0.875}Fe_{0.125}O_{2-\delta}$ surface, respectively. It is noteworthy that the reaction energies depend on the oxygen vacancy formation energies, for which $Ce_{0.875}Mn_{0.125}O_2$ < $Ce_{0.875}Fe_{0.125}O_2$ < CeO_2. This is the same as the ordering of the reaction energies. Thus, the generation of the reoxidized surface by NO_2 is most favorable on the CeO_2 surface because the oxygen vacancy formation energy is highest among those surfaces. Conversely, the $Ce_{0.875}Mn_{0.125}O_2$ surface has the lowest oxygen vacancy formation energy so that it is the least favorable surface for NO_2 reduction.

4. CONCLUSIONS

The structures and energies of NO_2 adsorption and reduction on ceria and M-doped CeO_2 (111) (M = Mn, Fe) surfaces have been studied by using periodic DFT calculations corrected with the on-site Coulomb interaction via a Hubbard term (DFT+*U*). The interactions can divide into two types of NO_2 adsorption:

dx.doi.org/10.1021/jp412417e | J. Phys. Chem. C 2014, 118, 10043−10052

Table 4. Energies for the Catalytic Oxidation of CO and Reduction of NO_2 on the Ceria-based (111) Surface

reaction	CeO_2	$Ce_{0.825}Mn_{0.125}O_2$	$Ce_{0.825}Fe_{0.125}O_2$
$CeO_2 + CO \rightarrow CeO_{2-\delta} + CO_2$	−1.22	−2.86	−2.89
$CeO_{2-\delta} + NO_2 \rightarrow CeO_2 + NO$	−0.77	0.65	0.49
$CO + NO_2 \rightarrow CO_2 + NO$	−1.99	−2.21	−2.40

physisorption and chemisorption. NO_2 physisorption is observed at the oxygen and metal center (Ce, Mn, and Fe) sites with adsorption energies of −0.11 to −0.16, −0.12 to −0.23, and −0.05 eV for NO_2−CeO_2, NO_2−$Ce_{0.875}Mn_{0.125}O_2$, and NO_2−$Ce_{0.875}Fe_{0.125}O_2$, while NO_2 prefers to bind to the oxide anions via the nitrogen (η^1-N) or bond to O and metal centers via bidentate adsorption mode (μ^2-N,O), leading to NO_2 chemisorption and the formation of nitrate-like species (NO_3^-) with adsorption energies of −0.99 to −1.09, −1.46 to − 1.99, and −1.32 to −1.64 eV. For the defective surfaces, NO_2 physisorption is observed only at the Ce top sites of $Ce_{0.875}Mn_{0.125}O_{2-\delta}$ and $Ce_{0.875}Fe_{0.125}O_{2-\delta}$ surfaces with adsorption energies of −0.15 eV ($Ce_{0.875}Mn_{0.125}O_{2-\delta}$) and −0.27 eV($Ce_{0.875}Fe_{0.125}O_{2-\delta}$). NO_2 molecule adsorbs at the oxygen vacancy site through one of its oxygen atoms, leading to two bidentate chemisorption modes: μ^2-N,O on M, vac with adsorption energies of −1.95, −0.89, and −1.23 eV for $CeO_{2-\delta}$, $Ce_{0.875}Mn_{0.125}O_{2-\delta}$ and $Ce_{0.875}Fe_{0.125}O_{2-\delta}$ (111) surfaces and μ^2-O,O on M, vac (−2.02, −0.97, and −1.35 eV). It should note that other NO_2 chemisorption can be found for the defective M-doped CeO_2 (111) surfaces with adsorption energy of −0.49 eV for $Ce_{0.875}Mn_{0.125}O_{2-\delta}$ and adsorption energies of −1.00 and −0.70 eV for $Ce_{0.875}Fe_{0.125}O_{2-\delta}$. Our calculations showed that NO_2 adsorbs more strongly on the stoichiometric M-doped CeO_2 surfaces compared with the undoped surface with the formation of an adsorbed nitrate-like (NO_3^-) species, whereas NO_2 adsorption is less stable at the oxygen vacancy site on the defective M-doped CeO_2 surfaces than on the defective undoped surface, forming nitrite-like species (NO_2^-). Analyses of calculated vibrational frequencies and Bader charges were carried out to characterize those species. The adsorption energies of NO_2 are proportional to the oxygen vacancy energies for stoichiometric surfaces, while those are disproportional to the oxygen vacancy energies for defective surfaces. For the NO_2 reduction reaction, the reaction energy is exothermic for $CeO_{2-\delta}$, whereas it is endothermic for $Ce_{0.875}Mn_{0.125}O_{2-\delta}$ and $Ce_{0.875}Fe_{0.125}O_{2-\delta}$. The reaction energies depends on the oxygen vacancy formation energies, for which $Ce_{0.875}Mn_{0.125}O_2$ < $Ce_{0.875}Fe_{0.125}O_2$ < CeO_2. The ready formation and the high stability of NO_2 chemisorption (NO_3^- species formation on the stoichiometric surfaces and NO_2^- species formation on the defective surfaces) suggest that ceria-based materials can be the potential of NO_x storage-reduction catalysts used for lean-burn engines. Compared with CO oxidation, pure CeO_2 is a better catalyst for NO_2 reduction, whereas doped CeO_2 is a better catalyst for CO oxidation, as shown in Table 4. However, the catalytic reaction of $CO + NO_2 \rightarrow CO_2 + NO$ in Table 4 is all exothermic so that the oxidation of CO to CO_2 and the reduction of NO_2 to NO is favored and that it is predicted to be very exothermic on doped CeO_2.

■ ASSOCIATED CONTENT

Supporting Information

Top view and side view of the optimized geometries of NO_2 physisorption on CeO_2 (111) surface, $Ce_{0.875}Mn_{0.125}O_2$ (111) surface, and $Ce_{0.875}Fe_{0.125}O_2$ (111) surface. Top view and side view of the optimized geometries of NO_2 physisorption and NO formation on $CeO_{2-\delta}$ (111) surface, $Ce_{0.875}Mn_{0.125}O_{2-\delta}$ (111) surface, and $Ce_{0.875}Fe_{0.125}O_{2-\delta}$ (111) surface. This material is available free of charge via the Internet at http://pubs.acs.org.

■ AUTHOR INFORMATION

Corresponding Author

*E-mail: htchen@cycu.edu.tw. Tel: +886-3-265-3324.

Notes

The authors declare no competing financial interest.

■ ACKNOWLEDGMENTS

We are grateful to (1) Ministry of Science and Technology, Taiwan, under Grant Numbers NSC 101-2113-M-033-009-MY3 and NSC 101-2632-M-033-001-MY2 and Taiwan National Center for Theoretical Sciences (NCTS) for the financial support and (2) National Center for High-performance Computing, Taiwan, for the computer time and facilities.

■ REFERENCES

(1) Feng, X. D.; Sayle, D. C.; Wang, Z. L.; Paras, M. S.; Santora, B.; Sutorik, A. C.; Sayle, T. X. T.; Yang, Y.; Ding, Y.; Wang, X. D.; et al. Converting Ceria Polyhedral Nanoparticles into Single-Crystal Nanospheres. *Science* **2006**, *312*, 1504−1508.

(2) Liao, L.; Mai, H. X.; Yuan, Q.; Lu, H. B.; Li, J. C.; Liu, C.; Yan, C. H.; Shen, Z. X.; Yu, T. Single CeO_2 Nanowire Gas Sensor Supported with Pt Nanocrystals: Gas Sensitivity, Surface Bond States, and Chemical Mechanism. *J. Phys. Chem. C* **2008**, *112*, 9061−9065.

(3) Liu, W. W.; Zhou, K. B.; Wang, L.; Wang, B. Y.; Li, Y. D. Oxygen Vacancy Clusters Promoting Reducibility and Activity of Ceria Nanorods. *J. Am. Chem. Soc.* **2009**, *131*, 3140−3141.

(4) Yuan, Q.; Liu, Q.; Song, W. G.; Feng, W.; Pan, W. L.; Sun, L. D.; Zhang, Y. W.; Yan, C. H. Ordered Mesoporous $Ce_{1-x}Zr_xO_2$ Solid Solutions with Crystalline Walls. *J. Am. Chem. Soc.* **2007**, *129*, 6698−6699.

(5) Gamarra, D.; Belver, C.; Fernández-Garcia, M.; Martínez-Arias, A. Selective CO Oxidation in Excess H_2 over Copper−Ceria Catalysts: Identification of Active Entities/Species. *J. Am. Chem. Soc.* **2007**, *129*, 12064−12065.

(6) Pozdnyakova, O.; Teschner, D.; Wootsch, A.; Kröhnert, J.; Steinhauer, B.; Sauer, H.; Toth, L.; Jentoft, F. C.; Knop-Gericke, A.; Paal, Z.; et al. CO Oxidation in Hydrogen (PROX) on Ceria-Supported Catalysts, Part I: Oxidation State and Surface Species on Pt/CeO_2 Under Reaction Conditions. *J. Catal.* **2006**, *237*, 1−16.

(7) Si, R.; Zhang, Y. W.; Li, S. J.; Lin, B. X.; Yan, C. H. Urea-Based Hydrothermally Derived Homogeneous Nanostructured $Ce_{1-x}Zr_xO_2$ (x = 0−0.8) Solid Solutions: A Strong Correlation between Oxygen Storage Capacity and Lattice Strain. *J. Phys. Chem. B* **2004**, *108*, 12481−12488.

(8) Trovarelli, A. *Catalysis by Ceria and Related Materials*; Imperial College Press: London, 2002.

(9) Namai, Y.; Fukui, K.; Iwasawa, Y. The Dynamic Behaviour of CH_3OH and NO_2 Adsorbed on CeO_2(111) Studied by Noncontact Atomic Force Microscopy. *Nanotechnology* **2004**, *15*, S49.

(10) Liu, G.; Gao, P.-X. A Review of NO_x Storage/Reduction Catalysts: Mechanism, Materials and Degradation Studies. *Catal. Sci. Technol.* **2011**, *1*, 552−568.

(11) Roy, S.; Baiker, A. NO_x Storage−Reduction Catalysis: From Mechanism and Materials Properties to Storage−Reduction Performance. *Chem. Rev.* **2009**, *109*, 4054−4091.
(12) Mars, P.; van Krevelen, D. W. *Special Suppl.* Oxidations Carried Out by Means of Vanadium Oxide Catalysts. *Chem. Eng. Sci.* **1954**, *3*, 41−59.
(13) Shapovalov, V.; Metiu, H. Catalysis by Doped Oxides: CO Oxidation by $Au_xCe_{1-x}O_2$. *J. Catal.* **2007**, *245*, 205−214.
(14) Chen, H.-T. First-Principles Study of CO Adsorption and Oxidation on Ru-Doped CeO_2(111) Surface. *J. Phys. Chem. C* **2012**, *116*, 6239−6246.
(15) Chen, H.-T.; Chang, J.-C. Computational Investigation of CO Adsorption and Oxidation on Iron-Modified Cerium Oxide. *J. Phys. Chem. C* **2011**, *115*, 14745−14753.
(16) Hsu, L.-C.; Tsai, M.-K.; Lu, Y.-H.; Chen, H.-T. Computational Investigation of CO Adsorption and Oxidation on Mn/CeO_2(111) Surface. *J. Phys. Chem. C* **2013**, *117*, 433−441.
(17) Rodriguez, J. A.; Jirsak, T.; Sambasivan, S.; Fischer, D.; Maiti, A. Chemistry of NO_2 on CeO_2 and MgO: Experimental and Theoretical Studies on the Formation of NO_3. *J. Chem. Phys.* **2000**, *112*, 9929−9939.
(18) Berner, U.; Schierbaum, K.; Jones, G.; Wincott, P.; Haq, S.; Thornton, G. Ultrathin Ordered CeO_2 Overlayers on Pt(111): Interaction with NO_2, NO, H_2O and CO. *Surf. Sci.* **2000**, *467*, 201−213.
(19) Symalla, M. O.; Drochner, A.; Vogel, H.; Philipp, S.; Göbel, U.; Müller, W. IR-study of Formation of Nitrite and Nitrate During NO_x-Adsorption on NSR-Catalysts-Compounds CeO_2 and BaO/CeO_2. *Top. Catal* **2007**, *42/43*, 199−202.
(20) Filtshchew, A.; Stranz, D.; Hess, C. Mechanism of NO_2 Storage in Ceria Studied using Combined *in situ* Raman/FT-IR Spectroscopy. *Phys. Chem. Chem. Phys.* **2013**, *15*, 9066−9069.
(21) Nolan, M.; Parker, S. C.; Watson, G. W. Reduction of NO_2 on Ceria Surfaces. *J. Phys. Chem. B* **2006**, *110*, 2256−2262.
(22) Galea, N. M.; Scanlona, D. O.; Morgana, B. J.; Watson, G. W. A GGA+U Study of the Reduction of Ceria Surfaces and their Partial Reoxidation through NO_2 Adsorption. *Mol. Simul.* **2009**, *35*, 577−583.
(23) Scanlon, D. O.; Galea, N. M.; Morgan, B. J.; Watson, G. W. Reactivity on the (110) Surface of Ceria: A GGA+U Study of Surface Reduction and the Adsorption of CO and NO_2. *J. Phys. Chem. C* **2009**, *113*, 11095−11103.
(24) Kresse, G.; Hafner, J. *Ab initio* molecular dynamics for liquid metals. *Phys. Rev. B* **1993**, *47*, 558−561.
(25) Kresse, G.; Furthmüller, J. Efficient Iterative Schemes for *ab initio* Total-Energy Calculations using a Plane-Wave Basis Set. *Phys. Rev. B* **1996**, *54*, 11169−11186.
(26) Blöchl, P. E. Projector Augmented-Wave Method. *Phys. Rev. B* **1994**, *50*, 17953−17979.
(27) Perdew, J. P.; Burke, K.; Ernzerhof, M. Generalized Gradient Approximation Made Simple. *Phys. Rev. Lett.* **1996**, *77*, 3865−3868.
(28) Perdew, J. P.; Chevary, J. A.; Vosko, S. H.; Jackson, K. A.; Pederson, M. R.; Singh, D. J.; Fiolhais, C. Atoms, molecules, solids, and surfaces: Applications of the Generalized Gradient Approximation for Exchange and Correlation. *Phys. Rev. B* **1992**, *46*, 6671−6687.
(29) Perdew, J. P.; Wang, Y. Accurate and Simple Analytic Representation of the Electron-Gas Correlation Energy. *Phys. Rev. B* **1992**, *45*, 13244−13249.
(30) Monkhorst, H. J.; Pack, J. D. Special Points for Brillouin-Zone Integrations. *Phys. Rev. B* **1976**, *13*, 5188−5192.
(31) Nolan, M.; Grigoleit, S.; Sayle, D. C.; Parker, S. C.; Watson, G. W. Density Functional Theory Studies of the Structure and Electronic Structure of Pure and Defective Low Index Surfaces of Ceria. *Surf. Sci.* **2005**, *576*, 217−229.
(32) Nolan, M.; Parker, S. C.; Watson, G. W. The Electronic Structure of Oxygen Vacancy Defects at the Low Index Surfaces of Ceria. *Sur. Sci.* **2005**, *595*, 223−232.
(33) Fabris, S.; de Gironcoli, S.; Baroni, S.; Vicario, G.; Balducci, G. Taming Multiple Valency with Density Functionals: A Case Study of Defective Ceria. *Phys. Rev. B* **2005**, *71*, 041102.
(34) Fabris, S.; Vicario, G.; Balducci, G.; de Gironcoli, S.; Baroni, S. Electronic and Atomistic Structures of Clean and Reduced Ceria Surfaces. *J. Phys. Chem. B* **2005**, *109*, 22860−22867.
(35) Dudarev, S. L.; Botton, G. A.; Savrasov, S. Y.; Humphreys, C. J.; Sutton, A. P. Electron-Energy-Loss Spectra and the Structural Stability of Nickel Oxide: An LSDA+U Study. *Phys. Rev. B* **1998**, *57*, 1505−1509.
(36) Chen, H.-T.; Choi, Y. M.; Liu, M.; Lin, M. C. A Theoretical Study of Surface Reduction Mechanisms of CeO_2(111) and (110) by H_2. *ChemPhysChem* **2007**, *8*, 849−855.
(37) Loschen, C.; Carrasco, J.; Neyman, K. M.; Illas, F. First-principles LDA+U and GGA+U study of cerium oxides: Dependence on the effective U parameter. *Phys. Rev. B* **2007**, *75*, 035115.
(38) Andersson, D. A.; Simak, S. I.; Johansson, B.; Abrikosov, I. A.; Skorodumova, N. V. Modeling of CeO_2, Ce_2O_3, and CeO_{2-x} in the LDA+U formalism. *Phys. Rev. B* **2007**, *75*, 035109.
(39) Chen, H.-L.; Chang, J.-C.; Chen, H.-T. Origin of Doping Effects on the Oxygen Storage Capacity of $Ce_{1-x}M_xO_2$ (M = Fe, Ru, Os, Sm, Pu). *Chem. Phys. Lett.* **2011**, *502*, 169−172.
(40) Chen, H.-T.; Chang, J.-C. Oxygen Vacancy Formation and Migration in $Ce_{1-x}Zr_xO_2$ Catalyst: A DFT+U Calculation. *J. Chem. Phys.* **2010**, *132*, 214702.
(41) Jiang, Y.; Adams, J. B.; Schilfgaarde, M. V. Density-Functional Calculation of CeO_2 Surfaces and Prediction of Effects of Oxygen Partial Pressure and Temperature on Stabilities. *J. Chem. Phys.* **2005**, *123*, 064701.
(42) Yang, Z. X.; Woo, T. K.; Baudin, M.; Hermansson, K. Atomic and Electronic Structure of Unreduced and Reduced CeO_2 Surfaces: A First-Principles Study. *J. Chem. Phys.* **2004**, *120*, 7741−7749.
(43) Lyons, D. M.; Ryan, K. M.; Morris, M. A. Preparation of Ordered Mesoporous Ceria with Enhanced Thermal Stability. *J. Mater. Chem.* **2002**, *12*, 1207−1212.
(44) Lyons, D. M.; McGrath, J. P.; Morris, M. A. Surface Studies of Ceria and Mesoporous Ceria Powders by Solid-State ^1H MAS NMR. *J. Phys. Chem. B* **2003**, *107*, 4607−4617.
(45) Mills, G.; Jönsson, H.; Schenter, G. Reversible Work Transition State Theory: Application to Dissociative Adsorption of Hydrogen. *Surf. Sci.* **1995**, *324*, 305−337.
(46) Henkelman, G.; Uberuaga, B. P.; Jönsson, H. A Climbing Image Nudged Elastic Band Method for Finding Saddle Points and Minimum Energy Paths. *J. Chem. Phys.* **2000**, *113*, 9901−9904.
(47) Kummerle, E. A.; Heger, G. The Structures of C−$Ce_2O_{3+\delta}$, Ce_7O_{12}, and $Ce_{11}O_{20}$. *J. Solid State Chem.* **1999**, *147*, 485−500.
(48) Murugan, B.; Ramaswamy, A. V.; Srinivas, D.; Gopinath, C. S.; Ramaswamy, V. Nature of Manganese Species in $Ce_{1-x}Mn_xO_{2-\delta}$ Solid Solutions Synthesized by the Solution Combustion Route. *Chem. Mater.* **2005**, *17*, 3983−3993.
(49) Gupta, A.; Kumar, A.; Waghmare, U. V.; Hegde, M. S. Origin of Activation of Lattice Oxygen and Synergistic Interaction in Bimetal-Ionic $Ce_{0.89}Fe_{0.1}Pd_{0.01}O_{2-\delta}$ Catalyst. *Chem. Mater.* **2009**, *21*, 4880−4891.
(50) Nolan, M. Molecular Adsorption on the Doped (110) Ceria Surface. *J. Phys. Chem. C* **2009**, *113*, 2425−2432.